

Glycerol steam reforming over ceria-zirconia supported metallic catalysts

Marcin Cichy

*Department of Chemical Technology, Institute of Chemical Sciences,
Faculty of Chemistry, Maria Curie-Skłodowska University in Lublin
Maria Curie-Skłodowska Sq. 3, 20-031 Lublin, Poland
e-mail: marcin.cichy@umcs.pl*

Glycerol is a main by-product of transesterification reaction of plants oils to its methyl esters which are used as a substitute or as an additive to diesel fuel. Still growing so-called biodiesel production leads to large amounts of glycerol fraction flooding the market. One of the possible ways of its utilization is steam reforming reaction which main product is synthesis gas containing high concentration of hydrogen for which is still growing demand. In this work four metallic (Ni, Pt, Ru and Re) catalysts supported on ceria-zirconia mixed oxides have been investigated in glycerol steam reforming reaction. All catalysts were well characterized by use of various physiochemical methods including electron microscopy. Catalytic activity test allowed to choose rhodium catalyst as the most favourable in the studied reaction.

1. INTRODUCTION

The world's energy demand is growing faster than the population. One of the ways to solve the problem of meeting these needs, against many objections (environmental, climate, anthropogenic causes of the greenhouse effect) addressed to the

current situation (~85% of energy from fossil fuels) is the increasing use of the so-called renewable energy sources. By cause of the availability of biomass in virtually every place in the world, it is a very important currently but also a future energy resource. In addition to the commonly used biomass combustion, in the second half of the 20th century began to use of some of its types (e.g. vegetable oils, cereals) for the production of liquid fuel products – biofuels (biodiesel, bioethanol).

Due to the rapid development of biodiesel production technology, the amount of waste glycerine fraction is constantly increasing. Over the past dozen or so years, interest in this raw material has increased significantly, including its utilization methods. In addition to the classical ways, such as tobacco, food, cosmetics, and pharmaceutical industries as well as the production of explosives, there are a whole range of new solutions leading to obtain valuable chemical products such as dehydration, oxidation, hydrogenation, esterification, etherification and processes for the production of epichlorohydrin and hydrogen [1–3].

The conversion of the glycerol waste fraction into syngas including the subsequent reaction of CO conversion with steam (WGS – Water Gas Shift reaction) seems to meet the hopes of managing any amount of this waste in a very useful direction, obtaining valuable products, i.e. synthesis gas and hydrogen. Glycerol steam reforming can generally be represented as a reaction leading to the formation of 7 moles of hydrogen and 3 moles of carbon dioxide from one mole of glycerol (1) [4]:



This process takes place in two stages. In the first stage, glycerol decomposes into carbon monoxide and hydrogen, which is in a sense a pyrolysis reaction, especially at high temperatures. On the other hand, the next reaction is followed by the water gas shift reaction (2, 3) [4].



The main task of glycerol steam reforming catalysts is to ensure the efficient course of glycerol decomposition reactions and the

subsequent WGS reaction with the simultaneous inhibition of undesirable methanation processes and the formation of carbon deposit. A review of literature data indicates that next to nickel, noble metals as an active phase and cerium oxides or ceria-zirconia as a supports are of great interest [5-10].

In this paper results of glycerol steam reforming reaction over four ceria-zirconia supported metal catalysts has been presented. Also physiochemical and structural properties of all catalysts as well as support were investigated.

2. EXPERIMENTAL

2.1. Catalysts preparation

To the dried $\text{CeO}_2\text{-ZrO}_2$ (CeZr) commercial support (Rhodia), grinded to 0.3-0.6 mm, nickel, platinum, ruthenium and rhodium were added by incipient wetness impregnation method using solutions of the following metal salts: nickel (II) nitrate (POCh Gliwice), chloroplatinic acid (POCh Gliwice), rhodium (III) chloride (Alfa Aesar) and ruthenium (III) chloride (Alfa Aesar). Catalysts precursors were dried at 70°C and then they were calcined in air at 400°C for 6 hours. Such prepared catalysts were denoted as: Ni/Ce-Zr, Pt/Ce-Zr, Ru/Ce-Zr, Rh/Ce-Zr, respectively.

2.2. Physiochemical and structural characterization

Catalysts and CeZr support physiochemical and structural properties were well characterized. Composition was determined by energy dispersion X-Ray spectroscopy (ED-XRF) using Canberra 1510 spectrometer (Canberra-Packard). Specific surface area of support and catalysts (after reduction) was determined on ASAP 2420M apparatus (Micromeritics Instrument Corporation). Surface area (S_{BET}) was calculated by the Brunauer, Emmett and Teller method. Whereas the pore volume (V_p), their average size (diameter, D_p) and the pore size distribution were determined from the desorption isotherm curve by the Barret-Joyner-Hallenda (BJH) method. The size of the active metal phase (Me) in the catalysts was determined by hydrogen chemisorption method using the ASAP 2020C analyzer (Micromeritics Instrument Corporation). The determinations were made at a temperature of 35°C (for Ni, Pt, Rh) or 100°C (for Ru).

Phase composition was determined by X-Ray diffraction method (XRD) using Empyrean diffractometer (PANalytical). Reducibility tests were carried out by the Temperature-Programmed Reduction (TPR) method using the Autochem II 2920 (Micromeritics Instrument Corporation), equipped with a TCD detector and system for generating low temperatures, fed with liquid nitrogen. Titan G2 60-300 High Resolution Scanning/Transmission Electron Microscope (HR S/TEM, FEI) was used to image catalyst samples. Samples mapping was performed in STEM mode, collecting the EDS spectrum from each location corresponding to map pixels, point by point.

2.3. Catalytic tests

Glycerol steam reforming reaction was performed in quartz tube flow reactor. 10 mg of catalyst sample was reduced in hydrogen stream at 800°C for 2 hours, prior to the reaction. Process was carried out in temperature range 800-650°C (50°C step) for 6 hours. Water/glycerol mixture with 9/1 molar ratio was delivered to reactor by syringe pump with speed of 2 cm³/h. After leaving reactor products stream was separated into gas and liquid fraction. Gaseous products were directly transported by carrier gas (He) to gas chromatograph equipped with TCD detector (Fisons GC-8030) and analysed for H₂, CO, CO₂, CH₄ and C₂H₄ content. Second fraction, containing unreacted glycerol and water as well as trace amounts of liquid products were collected and analyzed for glycerol content by using gas chromatograph equipped with FID detector (Shimadzu GC-2010).

3. RESULTS AND DISCUSSION

Table 1 presents physiochemical properties of CeZr support and catalyst studied.

The introduction of metals into the support and reduction of catalysts resulted in a decrease in the specific surface area. Small changes in the specific surface area of catalysts containing small amounts of Pt, Ru and Rh (1.3-1.6 wt.%) indicate that the main reason for the reduction in surface area in the nickel catalyst is the introduction of over 13 wt.% of Ni. Other quantities characterizing structural properties did not change significantly after the

introduction of various metals. The pore size distribution is shown in Figure 1.

Table 1. Physiochemical properties of CeZrO₂ support and catalyst studied.

Support/ Catalyst	Me content [wt.%] (Me = Ni, Pt, Ru, Rh)	S_{BET} [m ² /g]	V_p [cm ³ /g]	D_p [nm]
CeZr		50.0	0.14	9.5
Ni/CeZr	13.6	35.9	0.15	15.0
Pt/CeZr	1.6	48.5	0.19	13.0
Ru/CeZr	1.4	48.9	0.19	13.0
Rh/CeZr	1.3	48.5	0.19	13.0

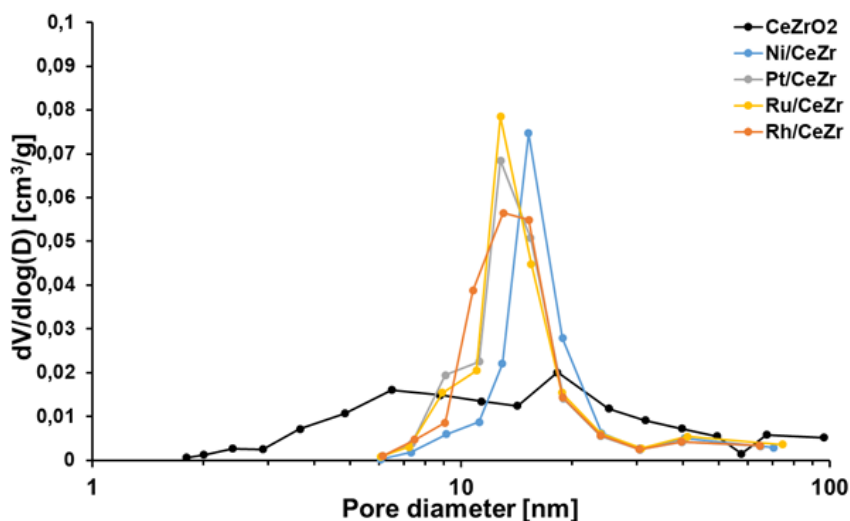


Fig. 1. Pore size distribution of the support and catalysts studied.

The diffractograms of CeZrO₂ supported catalysts are shown in Fig. 2. The Rhodia support turned out to be a solid solution of cerium and zirconium oxides with a composition of Ce_{0.62}Zr_{0.38}O₂ (ICDD: 01-075-9466). Analysis of individual diffractograms showed the presence of metal characteristic bands only in the following catalysts: Ni/CeZr – nickel (ICDD: 04-004-8734) and Ru/CeZr – ruthenium (ICDD: 04-007-8255). Such results of XRD examinations, due to the

low content of noble metals in catalysts, did not allow to determine the size of crystallites of metals other than nickel.

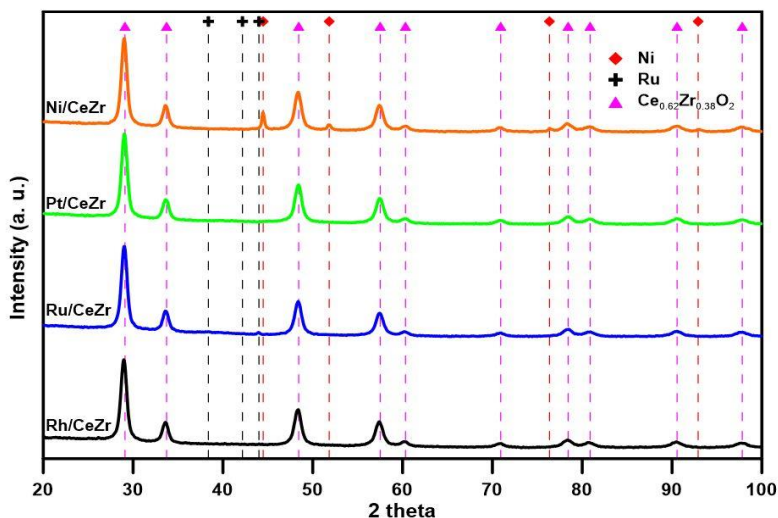


Fig. 2. XRD diffraction patterns of CeZrO_2 supported catalyst.

Only for Ni and Ru catalysts the phase composition was able to determine by Rietveld analysis method. Metal content was calculated as 24 and 2 wt.%, and $\text{Ce}_{0.62}\text{Zr}_{0.38}\text{O}_2$ phase as 76 and 98 wt.%, respectively.

Table 2 presents metal active surface, metal dispersion and average crystallite size obtained by various methods (chemisorption – d_H , XRD – d_X and STEM – d_M).

Table 2. Results of hydrogen chemisorption analysis and average crystallite size of catalysts studied.

Catalyst	S_H [m^2/g]	Me dispersion [%]	Average crystallite size [nm]		
			d_H	d_X	d_M
Ni/CeZr	1.2400	1.40	73	36	15.8
Pt/CeZr	0.0560	1.40	80	–	1.8
Ru/CeZr	0.0251	0.46	289	–	27.9
Rh/CeZr	0.8200	14.20	8	–	2.2

Hydrogen chemisorption studies have shown surprisingly low results for Pt and Ru catalysts. Many authors point out the difficulties with using the hydrogen chemisorption method to determine the surface size of noble metals on supports containing cerium oxide [e.g. 11, 12]. The possibility of hydrogen adsorption on CeO₂ [13], as well as the occurrence of the of hydrogen spillover phenomenon from noble metal on a support [11, 14] means that by using hydrogen chemisorption to determine the noble metal dispersion, can get overvalued results.

On the other hand, it has been shown that due to the possibility of occurrence, in catalysts containing CeO₂ (after reduction at elevated temperatures), the phenomenon of strong metal-support interactions (SMSI) [12], as the reduction temperature increases, the hydrogen/metal (H/M) ratio decreases with hydrogen chemisorption [11, 15].

Considering both described effects and high reduction temperature (800°C) used in these tests, it seems that in the case of Pt/CeZr and Ru/CeZr catalysts the effect of decreasing H/M ratio for hydrogen chemisorption prevailed.

However, for the Rh/CeZr catalyst using hydrogen chemisorption method, a result indicating high metal dispersion (~14%) was obtained. Literature data indicate that the use of rhodium chloride (RhCl₃) for catalyst synthesis reduces SMSI [14, 16, 17].

Based on S/TEM microscopic images, the crystallites size distributions of platinum, nickel, ruthenium and rhodium in tested catalysts were determined. For 112 Pt particles (dimensions from 0.8 nm to 3.1 nm), 11 Ni particles (from 5.55 nm to 24.10 nm), 43 Ru particles (from 9.6 to 82, 9) and 15 Rh particles (from 0.93 nm to 3.34 nm) mean crystallite sizes were determined as 1.8, 15.81, 27.9 and 2.2 nm, respectively (Table 2).

Figures 3-5 show presence of very small Pt and Rh crystallites and large Ni particles.

Figures 6 and 7 present STEM images and EDS maps of Pt/CeZr and Rh/CeZr catalysts showing the distribution of individual components and the dispersion of metal crystallites (Pt and Rh).

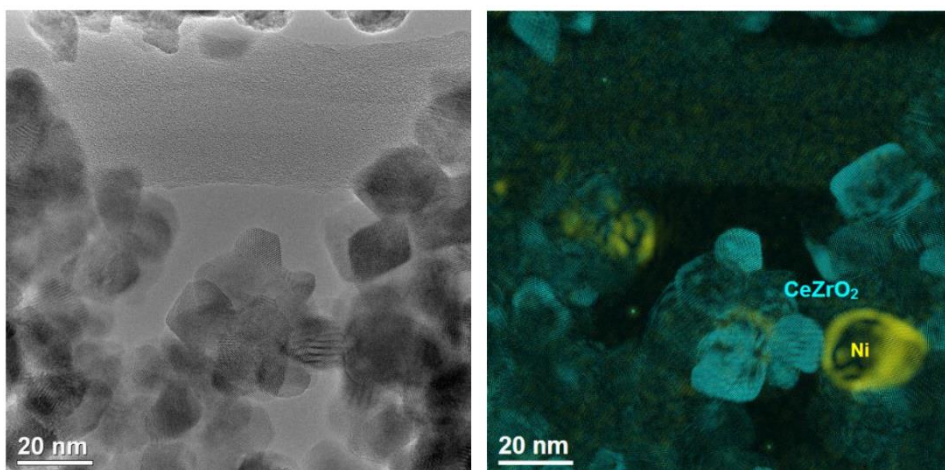


Fig. 4. HRTEM images of reduced Ni/CeZr catalyst.

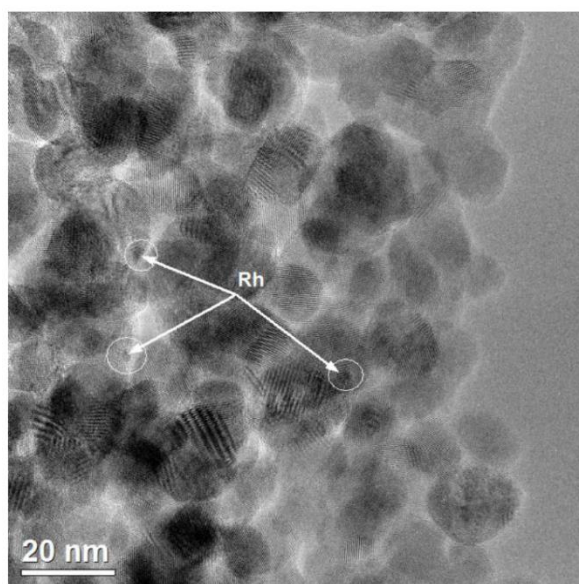


Fig. 5. HRTEM Image of reduced Rh/CeZr catalyst.

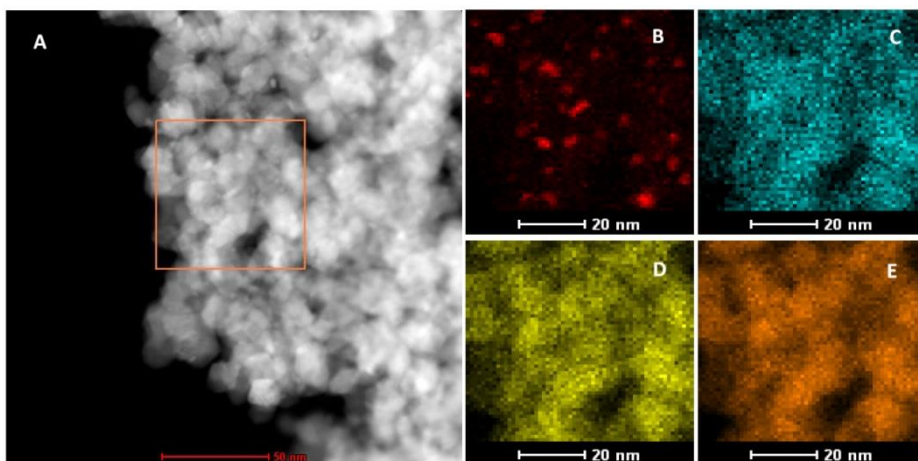


Fig. 6. STEM image (A) and EDS maps of Pt/CeZr catalyst (B - Pt, C - Ce, D - Zr, E - O₂).

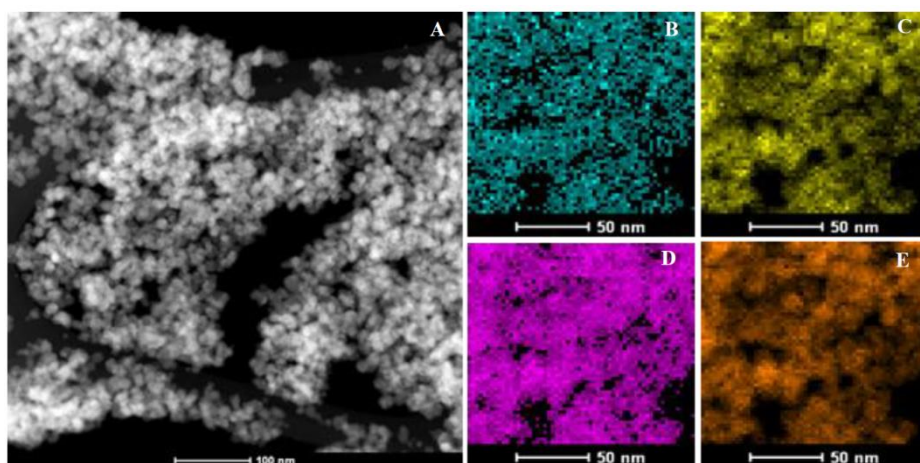


Fig. 7. STEM image (A) and EDS maps of Rh/CeZr catalyst (B - Rh, C - Ce, D - Zr, E - O₂).

To summarize the research on metal dispersion in Me/CeZr catalysts, it can be stated that all three methods indicate very low dispersion of Ru, electron microscopy and the XRD method indicate very high Pt dispersion and both hydrogen chemisorption and electron microscopy indicate high rhodium dispersion. Also all used techniques showed an average dispersion of nickel in a Ni/CeZr catalyst (Table 2).

Figure 8 presents reducibility curves of CeZr support and all four catalysts obtained by TPR method.

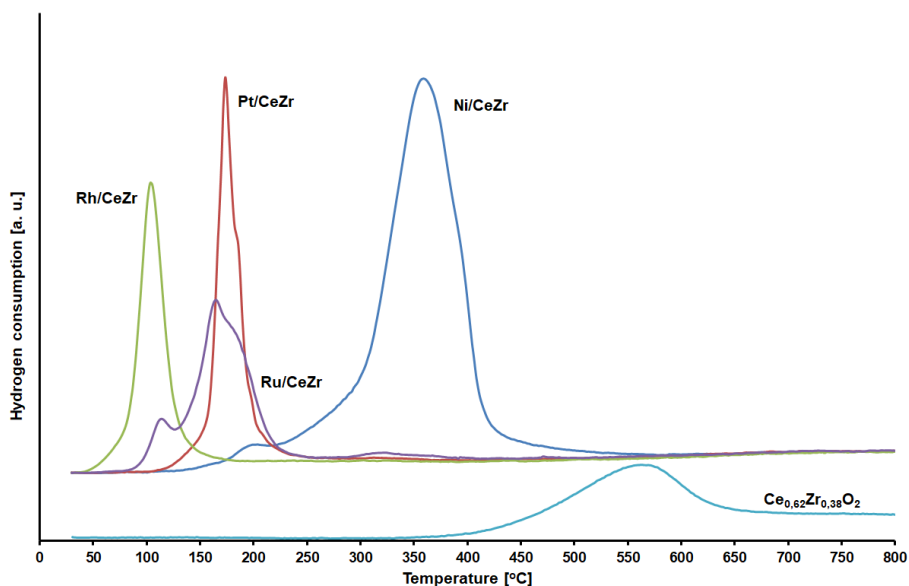


Fig. 8. TPR profiles of support and catalysts studied.

The $\text{Ce}_{0.6}\text{Zr}_{0.4}\text{O}_2$ support reduces with the maximum peak at 570°C .

For this phenomenon is probably responsible reduction of the surface layer of cerium oxide. However, no hydrogen consumption was observed on the TPR curves of the supported catalysts in this temperature range. The same situation was described in [18] for the $\text{Ce}_{0.75}\text{Zr}_{0.25}\text{O}_2$ support, for which the maximum reduction peak occurred at 581°C , and which did not appear when reducing the $\text{Pt}/\text{Ce}_{0.75}\text{Zr}_{0.25}\text{O}_2$ catalyst.

For co-precipitated $\text{Ce}_{0.7}\text{Zr}_{0.3}\text{O}_2$ support Sharma et al. [19] confirmed the presence of two reduction maxima at 546°C (main) and 761°C (weak), respectively. It can be seen, that despite the differences in composition and the conditions of synthesis and calcination temperatures, TPR profiles of both CeZrO_2 supported catalysts are very similar.

The course of NiO reduction in Ni/CeZr is typical for nickel containing catalysts. Its TPR profile can be divided into two maxima, one at $\sim 200^\circ\text{C}$ (NiO weakly bonded with support) and the other at $\sim 360^\circ\text{C}$ (reduction of NiO interacting with support).

The reduction of noble metal catalysts varies but in significantly lower temperatures. The TPR profile of platinum catalyst with one reduction peak at maximum temperature of $\sim 170^{\circ}\text{C}$ is similar to the Pt/Ce_{0.75}Zr_{0.25}O₂ catalyst reduction temperature described in work [18]. Rhodium oxide is easiest to reduce, with a single reduction peak with a maximum at $\sim 100^{\circ}\text{C}$. For much easier reduction of rhodium oxide on the Ce_{0.7}Zr_{0.3}O₂ than on Al₂O₃ support present results in work [19], where the reduction peaks maxima were found at 80 and 157 $^{\circ}\text{C}$, respectively.

The shape of the ruthenium catalyst reduction profile is more complex (three maxima). Similar reduction curves are described in work [20] for Ru/Ce_{0.75}Zr_{0.25}O₂ catalysts with variable ruthenium content. The shape of the presented curve for a catalyst with a similar Ru content is almost identical, but shifted towards higher temperatures.

Considering that the Ru/CeZr catalyst was prepared using RuCl₃, the first two maxima at ~ 120 and $\sim 170^{\circ}\text{C}$ can be attributed to ruthenium (III) chloride [21, 22] and ruthenium oxychloride [22, 23], respectively. This is likely due to the low calcination temperature of the catalyst (400°C) [23]. The third maximum ($\sim 200^{\circ}\text{C}$) seems to be associated with the reduction of RuO₂ [23, 24]. The low temperatures of reduction maxima observed for the Ru/CeZr catalyst can be the consequence of very low dispersion of Ru particles. This confirms the shift of the maximum reduction towards low temperatures shown in work [20], when ruthenium content in catalysts increases and dispersion decreases.

3.1. Catalysts performance

Me/CeZr catalysts activity is presented as glycerol conversion degree (X_{Gl}) (Fig. 9) and selectivity towards hydrogen (Fig. 10) and carbon containing gaseous products (Fig. 11) as function of temperature.

All catalysts showed high activity at 750 and 800 $^{\circ}\text{C}$. At 800 $^{\circ}\text{C}$, glycerol conversion rates ranged from 91% (Ni/CeZr) to 96% (Ru/CeZr). At these high reaction temperatures, a series of metal activities on the CeZrO₂ support were as follows: Ru>Rh>Pt>Ni (Fig. 9). Lowering reaction temperature increased the difference between the individual catalysts. The Ni/CeZr catalyst maintained high activity at 700 $^{\circ}\text{C}$ ($X_{\text{Gl}} = 85\%$), while rhodium and ruthenium

catalysts were characterized by high activity (compared to other samples) at 650°C ($X_{GI} > 70\%$).

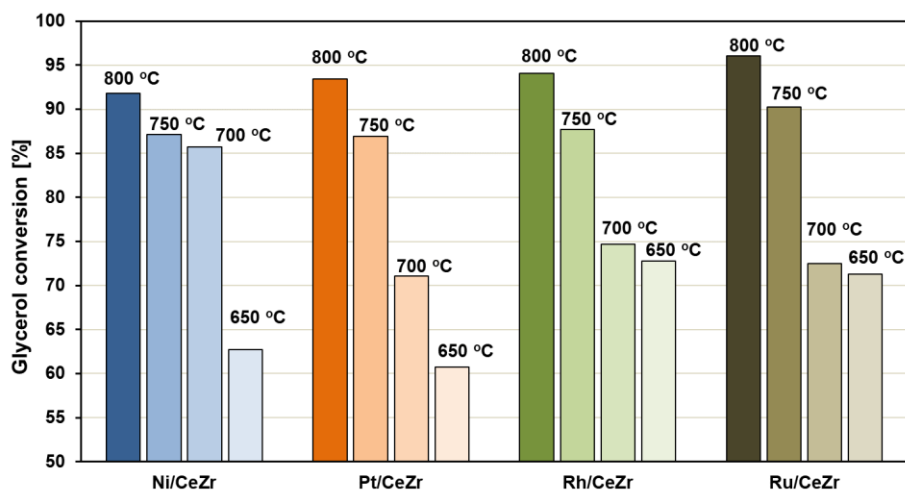


Fig. 9. Glycerol conversion over Me/CeZr catalysts in 650-800°C temperature range.

The results of hydrogen selectivity (Fig. 10) showed that the highest selectivity, above 45%, for all catalysts was obtained at a temperature of 800°C. The best catalyst turned out to be Rh/CeZr, which in the entire temperature range was characterized by the highest selectivity (46–59%).

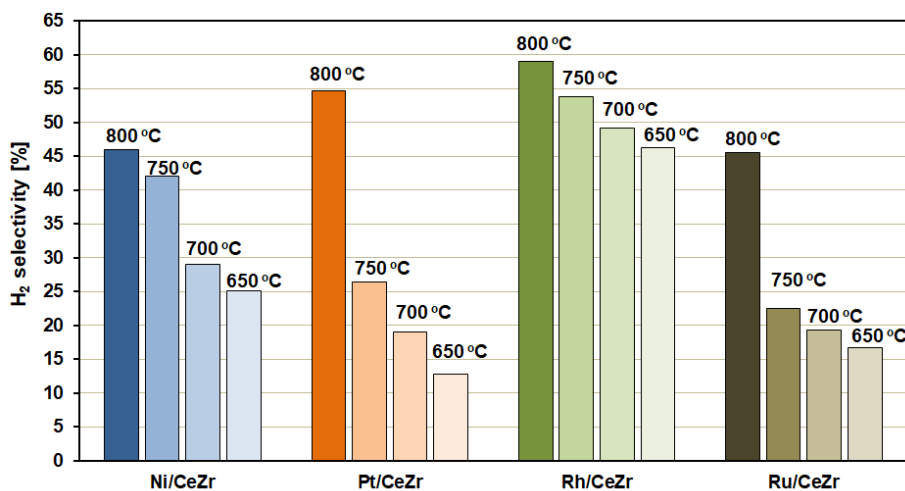


Fig. 10. Me/CeZr catalysts hydrogen selectivity in 650-800°C temperature range.

The selectivity for hydrogen decreased very quickly when the temperature was reduced for Pt/CeZr and Ru/CeZr. The nickel catalyst showed intermediate properties, more favorable than Pt and Ru, but worse than the Rh one.

The type of metal used also had a significant impact on carbon products selectivity (Fig. 11). The highest selectivity to carbon dioxide, suggesting high activity in the water-gas shift reaction (WGS) corresponding to the amount of hydrogen produced, was obtained for rhodium catalyst. Lowering the reaction temperature decreased CO₂ selectivity, especially for Pt and Ru catalysts.

At the same time, with the reaction temperature drop, increased hydrocarbons concentration in the gas stream leaving the reactor was observed. The smallest amounts of methane and ethylene were formed on the Rh/CeZr catalyst. A slight increase in selectivity to CH₄ (6.5 → 10%) and C₂H₄ (1.5 → 5.5%) was found when the temperature drops (800 – 650 °C). For the Pt/CeZr catalyst, the ethylene selectivity increased from 3 to over 10%. Similar results were obtained for other catalysts.

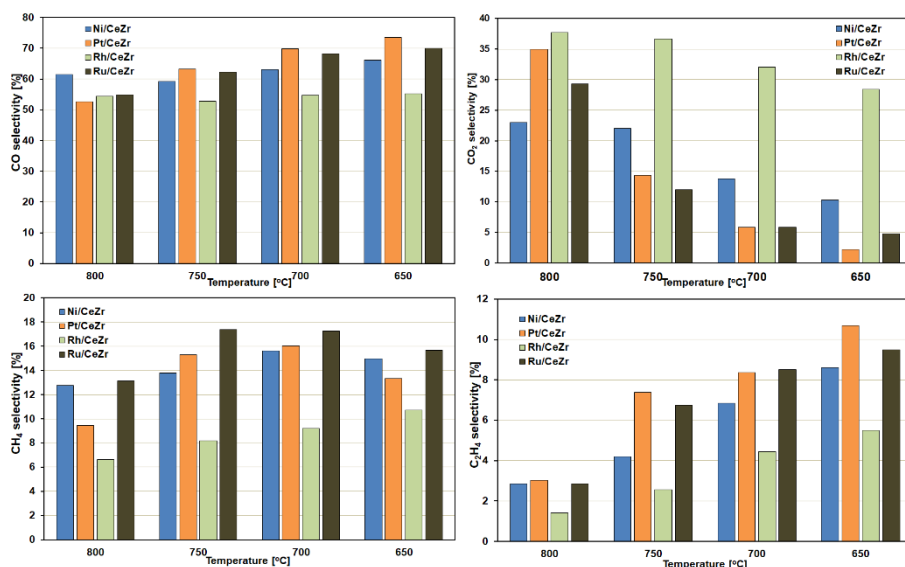


Fig. 11. Me/CeZr catalysts carbon containing products selectivity in 650-800°C temperature range.

In the reaction products, next to methane, ethylene was found, and their amounts decreased with increasing temperature. The formation of hydrocarbons is not favourable because hydrogen is

consumed in these reactions [25]. Not only thermodynamic considerations, but also experimental studies have shown that an increase in temperature reduces the amount of methane produced [25]. Explanation of the causes and effects of the presence or absence of hydrocarbons other than methane (mainly ethane and ethylene) in glycerol steam reforming products is not of much interest in published papers. Much more attention is paid to the diversity of both the composition and the amount of oxygenated products of the reaction, which depends to a large extent on the temperature, as well as the catalyst and the steam/glycerol ratio [5, 26–29].

In certain publications, described tests carried out under different conditions and over different catalysts did not show the presence of hydrocarbons in products other than methane [29–34]. In others, they will be from trace [27, 35] to significant amounts [24, 36]. In some researches, as in this study, only the presence of ethylene was found [26, 37–39]. Valliyappan et al. [38] on the Ni/Al₂O₃ catalyst at 800 °C found only CO, H₂, CO₂, CH₄ and C₂H₄ in the gaseous reaction products. The amount of ethylene decreased with increasing steam/glycerol ratio.

With the presence of ethylene [26, 37], as well as the formation of condensing products (mainly hydroxyacetone) [26], the possibility of catalyst deactivation is associated.

CONCLUSIONS

Four metallic catalysts supported on mixed ceria-zirconia oxide were investigated in glycerol steam reforming reaction. The obtained results justify the statement that among the tested catalysts, the most advantageous properties in the studied reaction showed Rh/CeZr catalyst. It provided the highest reactivity of substrates, the highest selectivity to hydrogen and carbon dioxide, and the lowest to hydrocarbons. Among other metals, nickel deserves attention, because although it turned out to be slightly inferior to platinum, it is definitely cheaper than precious metals.

REFERENCES

- [1] Ch. H. Zhou, H. Zhao, D. S. Tong, L. M. Wu, W. H. Yu, *Catal. Rev. Sci. Eng.*, **55**, (2013), 369-453.
- [2] Z. Gholami, A. Z. Abdullah, K-T. Lee, *Renew. Sust. Energ. Rev.*, **39**, (2014), 327-341.
- [3] M. Cichy, Nowe kierunki wykorzystania glicerolu w przemyśle chemicznym, w Adsorbenty i katalizatory. Wybrane technologie a środowisko, (Ed. J. Ryczkowski), Uniw. Rzeszowski, Rzeszów, (2012), 309-322.
- [4] K. N. Papageris, G. Siakavelas, N. D. Charisiou, D. G. Avraam, L. Tzounis, K. Kousi, M. A. Goula, *Fuel. Process. Technol.*, **152**, (2016), 156-175.
- [5] Y-Ch. Lin, *Int. J. Hydrogen Energ.*, **38**, (2013), 2678-700.
- [6] M. Cichy, T. Borowiecki, *Przem. Chem.*, **88**, (2009), 995-1005.
- [7] T. Hirai, N-O. Ikenaga, T. Miyake, T. Suzuki, *Energ. Fuel*, **19**, (2005), 1761-2.
- [8] M. Slinn, F. Pompeo, G. Santori, N. N. Nichio, *Int. J. Hydrogen Energ.*, **35**, (2010), 8912-20.
- [9] K. Kendall, C. Mallon, J. Andrews, *Bioresour. Technol.*, **99**, (2008), 5851-8.
- [10] S. Adhikari, S. D. Fernando, S. D. F. To, R. M. Bricka, F. H. Steele, A. Haryanto, *Energ. Fuel*, **22**, (2008), 1220-6.
- [11] S. Bernal, J. J. Calvino, M. A. Cauqui, J. M. Gatica, C. Larese, J. A. Perez-Omil, J. M. Pintado, *Catal. Today*, **50**, (1999), 175-206.
- [12] S. Komai, Y. Yazawa, A. Satsuma, T. Hattori, *J. Jpn. Petrol Inst.*, **48**, (2005), 173-7.
- [13] P. P. Silva, F. A. Silva, L. S. Portela, L. V. Mattos, F. B. Noronha, C. E. Hori, *Catal. Today*, **107-108**, (2005), 734-40.
- [14] S. D. Angeli, L. Turchetti, G. Monteleone, A. A. Lemonidou, *Appl. Catal. B*, **181**, (2016), 34-46.
- [15] C. Leitenburg, A. Trovarelli, J. Kaspar, *J. Catal.*, **166**, (1997), 98-107.
- [16] S. Bernal, F. J. Botana, J. J. Calvino, M. A. Cauqui, G. A. Cifredo, A. Jobacho, J. M. Pintado, J. M. Rodríguez-Izquierdo, *J. Phys. Chem.*, **97**, (1993), 4118-123.
- [17] D. I. Kondarides, X. E. Verykios, *J. Catal.*, **174**, (1998), 52-64.
- [18] S. M. de Lima, A. M. Silva, U. M. Graham, G. Jacobs, B. H. Davis, L. V. Mattos, F. B. Noronha, *Appl. Catal. A*, **352**, (2009), 95-113.
- [19] P. K. Sharma, N. Saxena, P. K. Roy, A. Bhatt, *Int. J. Hydrogen Energ.*, **41**, (2016), 6123-33.
- [20] J. Chen, Ch-Ch. Yao, Y. Zhao, P. Jia, *Int. J. Hydrogen Energ.*, **35**, (2010), 1630-42.
- [21] V. A. Mazzieri, M. R. Sad, C. R. Vera, C. L. Pieck, R. Grau, *Quím. Nova*, **33**, (2010), 269-72.

- [22] V. A. Mazziere, F. Coloma-Pascual, A. Arcoya, P. C. L'Argentiere, N. S. Figoli, *Appl. Surf. Sci.*, **210**, (2003), 222-30.
- [23] A. Bossi, F. Garbassi, A. Orlandi, G. Petrini, L. Zanderighi, *Stud. Surf. Sci. Catal.*, **3**, (1979), 405-16.
- [24] P. G. J. Koopman, A. P. G. Kieboom, H. van Bekkum, *J. Catal.*, **69**, (1981), 172-9.
- [25] S. Adhikari, S. Fernando, A. Haryanto, *Energ. Fuel*, **21**, (2007), 2306-10.
- [26] L. M. Martinez T, M. Araque, J. C. Vargas, A. C. Roger, *Appl. Catal. B*, **132-133**, (2013), 499-510.
- [27] A. Iriondo, V. L. Barrio, J. F. Cambra, P. L. Arias, M. B. Guemez, M. C. Sanchez-Sanchez, R. M. Navarro, J. L. G. Fierro, *Int. J. Hydrogen Energ.*, **35**, (2010), 11622-33.
- [28] I. N. Buffoni, F. Pompeo, G. F. Santori, N. N. Nichio, *Catal. Comm.*, **10**, (2009), 1656-60.
- [29] L. P. R. Profeti, E. A. Ticianelli, E. M. Assaf, *Int. J. Hydrogen Energ.*, **34**, (2009), 5049-60.
- [30] A. Iriondo, V. L. Barri, J. F. Cambra, P. L. Arias, M. B. Guemez, R. M. Navarro, M. C. Sanchez-Sanchez, J. L. G. Fierro, *Top. Catal.*, **49**, (2008), 46-58
- [31] Ch. D. Dave, K. K. Pant, *Renew. Energ.*, **36**, (2011), 3195-202.
- [32] Ch. K. Cheng, S. Y. Foo, A. A. Adesina, *Ind. Eng. Chem. Res.*, **49**, (2010), 10804-17.
- [33] Ch. K. Cheng, S. Y. Foo, A. A. Adesina, *Catal. Today*, **178**, (2011), 25-33.
- [34] S. M. Swami, M. A. Abraham, *Energ. Fuels*, **20**, (2006), 2616-22.
- [35] A. M. D. Douette, S. Q. Turn, W. Wang, V. I. Keffer, *Energ. Fuel*, **21**, (2007), 3499-504.
- [36] E. A. Sanchez, M. A. D'Angelo, R. A. Comelli, *Int. J. Hydrogen Energ.*, **35**, (2010), 5902-7.
- [37] (2010), 5902-7.
- [38] M. L. Dieuzeide, M. Jobbagy, N. Amadeo, *Catal. Today*, **213**, (2013), 50-7.
- [39] T. Valliyappan, D. Ferdous, N. N. Bakhshi, A. K. Dalai, *Top. Catal.*, **49**, (2008), 59-67.
- [40] L. F. Bobadilla, A. Alvarez, M. Dominguez, F. Romero-Sarria, M. A. Centeno, M. Montes, J. A. Odriozola, *Appl. Catal. B*, **123-124**, (2012), 379-90.